Powder processing and characterisation of a quinary Ni-Mn-Co-Sn-Cu Heusler alloy

Riaz Ahamed*, Reza Ghomashchi, Zonghan Xie and Lei Chen*

School of Mechanical Engineering, University of Adelaide, Adelaide SA 5005

Paul Munroe and Song Xu

School of Materials Science and Engineering, University of New South Wales, Sydney NSW 2052

* Corresponding authors: riazahamed.ahamedkhan@adelaide.edu.au; lei.chen@adelaide.edu.au

Abstract

Ni-Co-Mn-Sn-Cu alloys were sintered from elemental powders at a temperature of 1050°C for 24 h. The resulting microstructures and physical properties were characterised by differential scanning calorimetry, X-ray diffraction, optical/electron microscopy and SQUID magnetometry. The new alloys exhibited a distinct martensitic transformation when cooled to room temperature. The presence of Cu in the powders moved the transformation temperature toward a higher value. The findings of this study demonstrate that the powder processing could be used to replace time-consuming arc/induction melting process in the development of high performance Heusler alloys at a lower cost.

Keywords: Heusler alloys; Powder processing; Microstructure, Martensite; Magnetic behaviour.

1. Introduction

Heusler alloys have attracted considerable interest due to their multiferroic attributes [1]. Often described as X_2YZ (X, Y – transition metals and Z – main group element), these alloys usually possess two of three ferroic characteristics - ferromagnetism, ferroelectricity and ferroelasticity, making them attractive functional materials for various applications [2]. What makes them multiferroic and therefore multifunctional is a phase transformation from austenite (at high temperatures) to martensite (at low temperatures) that occurs at a temperature below their Curie temperatures . This is also accompanied by a magnetic transition that changes the magnetic order of the phases [3]. For Heusler alloys martensitic transformation can occur over a range of temperature [4-7]. It can also be induced by the application of a magnetic field. The application of magnetic field may reduce martensite starting temperature and therefore cause reverse martensitic transformation by forming the high temperature ferromagnetic phase. Both structural and magnetic properties become strongly coupled to one another, giving rise to properties such as magnetic shape memory effect [8], magneto-caloric effect [9-11], magneto-resistance [7, 12] and direct conversion of heat into electricity [13].

Quite important in the study of Heusler alloys is the difference in magnetisation between the martensitic and austenitic phases, the larger the gap is, the better it is for driving structural transformation by application of magnetic fields. The field induced reverse martensitic transformation adds further to the functionality of the materials such as a large inverse magneto-caloric effect, giant strain and giant magneto-resistivity [14]. The alloy chemistry and atomic arrangement within crystal structure play an important role in phase transformation and resultant magnetization. A large difference in magnetisation between the phases is realised by the addition of Co to the Ni-Mn-Sn alloy [14] to replace Ni or Mn. Since Co has a higher magnetic moment than Ni [15], substitution of Ni with Co lowers the martensitic transformation temperature (M_s), while at the same time increases the Curie temperature (T_c). On the other hand, substitution by Co for Mn increases both M_s and T_c [16]. Addition of other elements such as Cu, too, has the

effect of changing the martensitic transformation temperature depending on whether it is substituted for Ni or Mn [17, 18]. For example, the substitution of Cu for Mn in $Ni_{50}Mn_{34}In_{16}$ ($Ni_{50}Mn_{34-x}Cu_xIn_{16}$) showed an increase in martensitic transition temperature along with a drop in Curie temperature [19]. However addition of Cu has not been shown to bring about a large difference in magnetisation between phases as Co does [17, 18].

It is common to synthesize Heusler alloys by arc/induction-melting of high purity elements in a controlled environment. The alloy casts are usually remelted over several times to improve homogeneity and reheated and kept at high temperatures (normally 80% of the melting point) for up to several days before quenching in ice water [20]. The rationale behind such prolonged treatment is to ensure a uniform distribution of constituent elements and the formation of fully martensitic structure at room temperature. Another technique used is to prepare the alloy ribbons by melt-spinning through a rapid solidification process. While the melt-spinning could bring about advantages like increased solid solubility limits and refinement of microstructure [21], it is difficult to prepare bulk materials and limits its application.

Powder metallurgy (P/M) is relatively simple material processing technique, where alloy composition can be tailored for specific application with minimum waste. Although the P/M process has been employed for fabrication of conventional shape memory alloys [22-28], it has been less common in the synthesis of ferromagnetic shape memory (Heusler) alloys. Furthermore, very few P/M fabrications reported in the literature used costly alloy powders rather than simple elemental powders. For example, spark plasma sintering (SPS), pressure-less sintering (PLS) and solid state replication were used to consolidate alloy powders of $Ni_{43}Co_7Mn_{39}Sn_{11}$, to explore the martensitic and magnetic properties usually found in cast alloys [29-31]. One advantage of P/M route is the control of porosity, which affects the ductility and shape recovery (memory) characteristics of these alloys [31].

Since no report can be found on the synthesis of Heusler materials by P/M using elemental powders, there is a practical need to explore the P/M routes in fabricating high performance Heusler alloys at low costs. This work reports on powder processing, microstructural development including phase transformation, magnetisation behaviour and the energy conversion function of quinary Ni-Mn-Co-Sn-Cu alloys prepared using elemental powders. The advantage of this method is discussed when compared to alloys prepared by melting.

2. Experimental procedure and sample preparation

The powder mixture was prepared with a starting stoichiometric composition of $Ni_{45}Mn_{40}Co_5Sn_{10}$ [13] reported for cast alloy that exhibited attractive martensitic and magnetic behaviour. Commercial purity elemental powders of nickel, manganese, cobalt and a mixture of tin and copper (2.5 wt.%) were used. The size distribution of the as-received elemental powders is given in Fig. 1 analysed using laser diffraction particle size analyser (Mastersizer 2000, Malvern Instruments, UK). The mean size for all powders is given in Table 1. The SEM micrographs in Fig. 2 provide an indication of powder morphology and size including some degree of agglomeration of the elemental powders.

Table 1. Powder particle size.

Powder	Ni/μm	Mn/μm	Sn-Cu/μm	Co/nm
Volumetric mean/D[4,3]	23.8	20.6	37.2	4029 (Z-Ave)

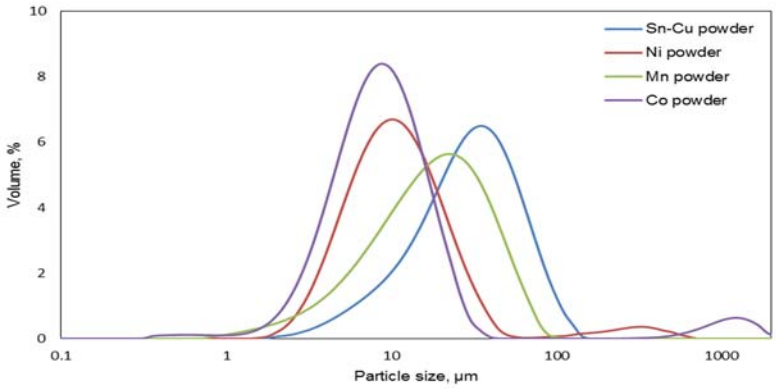

Fig. 1. Particle size distribution of constituent powders.

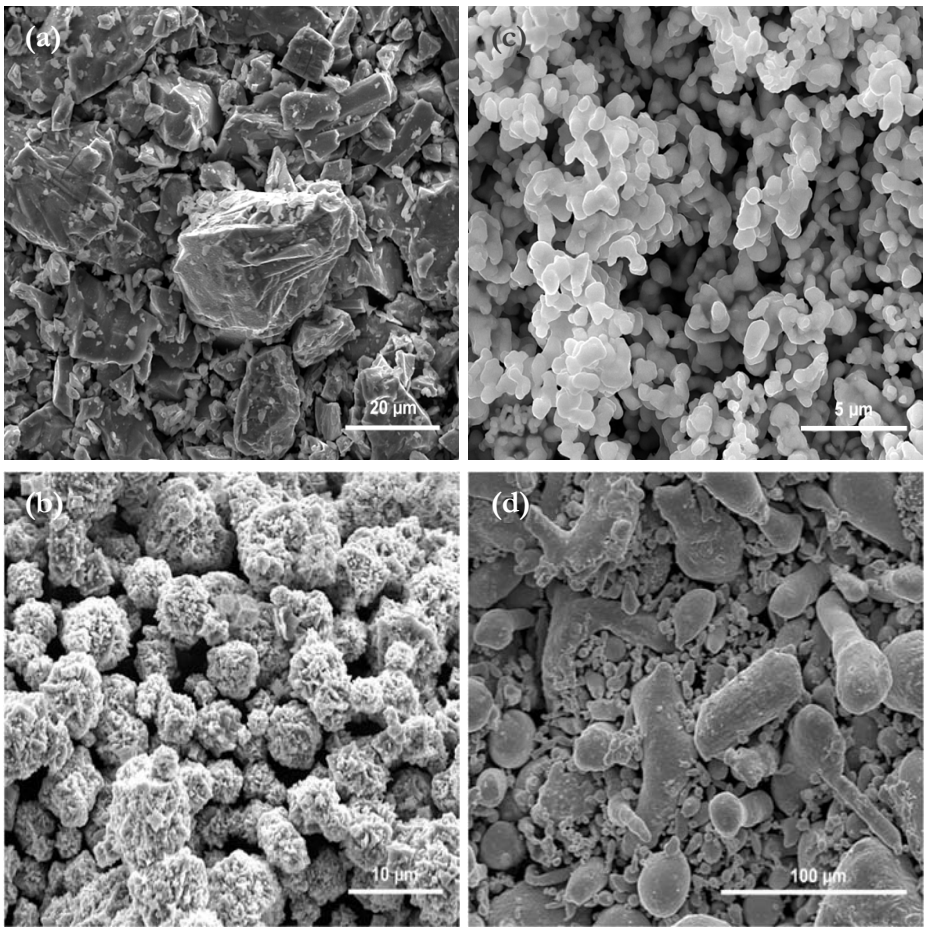

Fig. 2. SEM micrographs to show the morphology of (a) Mn (b) Ni (c) Co and (d) Sn-Cu powders.

The powders were carefully weighed and blended with an organic binder in a cylindrical mixer for 3 hours to render a good mixing. Following the mixing, the powders were compacted in a double action press at a maximum load of 70 kN to produce cylindrical compacts of 11 mm

diameter. The green compacts were sintered at 1050°C for 24 hours in a high temperature resistance heating tube furnace using an Ar atmosphere. The compacts were first heated at a heating rate of 5°C/min to 400°C, held for 30 minutes to burn off the binder and then ramped up to the sintering temperatures at the same rate.

For the microstructural analysis of as-sintered alloys, samples were cut using a slow speed diamond saw with surfaces prepared using an automatic polisher (Tegramin-25, Struers, Denmark). The etchant used was Kalling's reagent (50 ml HCl, 50 ml CH_3OH and 2-5 g $CuCl_2$). The microstructure and composition of the as-sintered samples were evaluated using FESEM (Quanta 450 FEG, USA) and electron microprobe (SXFive, CAMECA, France) with both EDS and WDS attachments. The formation of phases were confirmed by XRD (PANalytical Empyrean) using Cu-Kα radiation. The microstructure of the as-sintered specimens was also investigated by a transmission electron microscope (FEG-TEM, Philips CM200) operating at 200 KV. The samples used for TEM observation were prepared by a dual-beam focused ion beam system (FIB, XT Nova Nanolab 200), using a sample preparation method described elsewhere [32].

The phase transformation temperatures were measured using differential scanning calorimeter (Mettler-Toledo TGA/DSC) within the temperature range of 20 – 400°C at heating and cooling rates of 5°C/min. The magnetisation behaviour of the alloys was studied within a temperature range of 0 – 400 K under an applied magnetic field of 100 Oe using a superconducting quantum interference device (SQUID) magnetometer. Standard zero-field-cooled (ZFC), field-cooled (FC) and field-heated protocols were followed.

To demonstrate the use of the alloy in energy conversion, an identical device similar to the one used in was designed, shown in Fig. 3. A neodymium permanent magnet of 70 mm diameter and

15 mm thickness was used. Two coils of copper were used whose specifications are shown in Table 2.

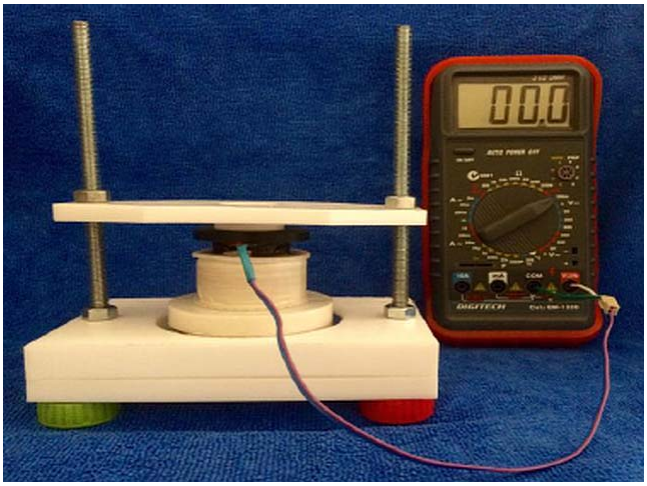

Fig. 3. Device used for energy conversion

Table 2. Specifications of coils

Coil	Turns	Wire diameter/mm	Outside diameter/mm	Inside diameter/mm	Height of coil/mm
Copper	4000	0.15	38	16	26
Copper	8000	01.5	38	19	20

A digital multimeter set to 200 mV DC was used to measure the voltage. Temperature changes were recorded using a thermal imager focussed onto the top of the coil. IRBIS3 Plus was used to analyse the images from the imager. The sample was heated to 400°C and then cooled differently using water and ice packs

3. Results and discussion

The volumetric mean diameter D[4,3] values of nickel, manganese powders and tin-copper mixture are ~23 μm, ~20.6 μm and ~37.2 μm respectively. The Z-average value of cobalt powder is ~4 μm. As expected, there is some degree of agglomeration of constituent powders that may affect the density of green compacts. The green density averaged around 70% of the theoretical density for the applied pressure of ~735 MPa. The measured density of the sintered specimens

was around 90% of the theoretical density after being kept for 24 hours at 1050°C. An EDS line scan shown in inset, between points 1 and 2 in the main panel of Fig. 4(a), confirms a uniform distribution of Mn, Ni, Co and Sn within the bulk alloy. The increased density is an indication of an effective diffusion amongst the particles of the constituent powders that helped close down the pores in between, Fig. 4(b) & (c). The microprobe analysis of the as-sintered specimens, as shown in Table 3, confirmed the alloy sample composition matches the design very well.

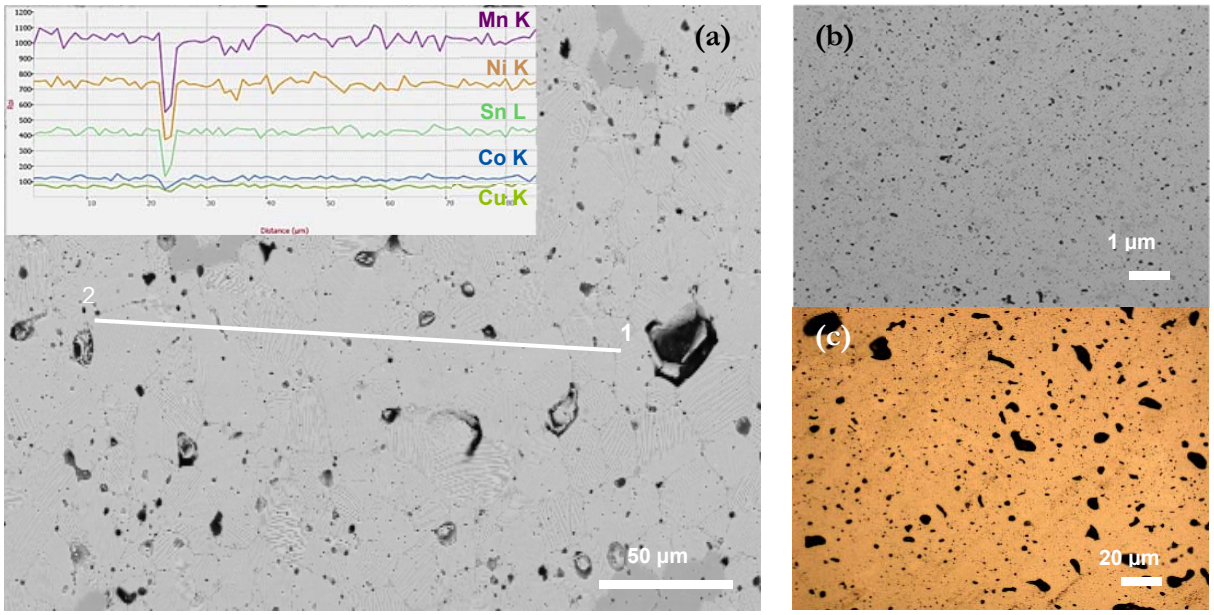

Fig. 4. (a) Inset shows an EDS line scan between points 1 & 2 (main panel) showing uniform distribution of constituent elements (b) SEM and (c) optical micrographs of the as-sintered specimen showing the distribution and morphology of the pores.

Table 3. Microprobe analysis of alloy composition of the as-sintered specimens.

Ni/at%	Mn/at%	Co/at%	Sn/at%	Cu/at%	Total
44.3	40.4	5.2	7.7	2.4	100

The optical and SEM micrographs of Fig. 5 provide a detailed view of the microstructural features in the sintered alloys. The formation of 'grains' or colonies bearing a clear martensitic morphology can be clearly seen in Fig. 5(a). The backscatter electron micrographs in Fig. 5(b) & (c), reveal the presence of the martensitic grains along with a bulky dark grey phase that have the distinct feature of intermetallics, both phase compositions are summarised in Table 4. In addition, a small number of little spongy-like phase, shown by black arrows in Fig. 5(b), was detected near the pores, whose composition is also given in Table 4. The spongy phase appears to be Sn-rich, while the bulky dark grey phase is rich in Co with a trace amount of Sn in solution. The formation of the spongy phase may be due to that the low melting point Sn flowed through the green compact at the early stage of sintering and accumulated within the pores. Dark regions which are rich in Co may have resulted from the agglomeration of Co particles, which had the smallest particle size, probably due to inadequate mixing. However, it is quite clear that more than 95% of the region are made of martensite phase as seen in Fig. 5(a).

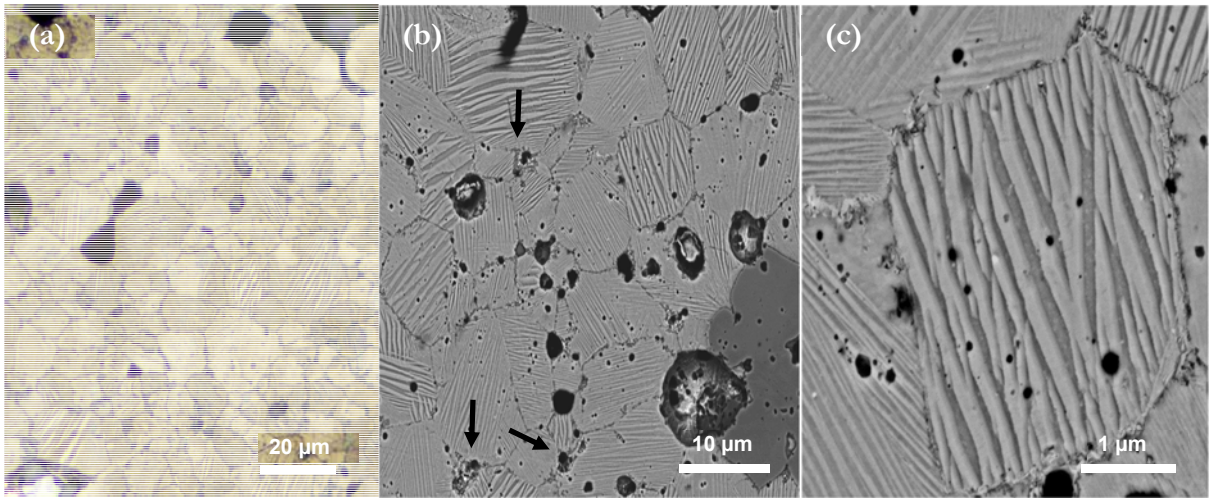

Fig. 5. Optical and backscatter electron micrographs to show the development of Heusler alloy synthesis

Table 4. Composition of micro-constituents determined by EDS

	Ni/at%	Co/at%	Mn/at%	Sn/at%	Cu/at%	Total
Martensitic grains	44.4	5.1	40.9	7.5	2.2	100
Spongy phase	43.8	5.1	37.8	10.2	3.2	100
Dark grey intermetallics	43.9	11.0	41.0	1.1	2.9	100

Furthermore, TEM studies were carried out to examine compositional variations across the martensitic laths and also provide information on the degree of homogeneity across entire grains. The main panel of Fig. 6 a) shows a twinned structure with martensitic laths evenly distributed. The compositional map of the thin section which confirms the uniform distribution of alloy elements is seen in the inset of Fig. 6 a). An EDS spectrum is shown in Fig. 6 b) for the points marked in the inset of Fig. 6 b).

The indication of martensite formation shows the potential of the P/M for the synthesis of Heusler alloys. To identify the martensitic structure and other phases which may form, XRD analysis of the specimen is shown in Fig. 7(a), in which the peaks are indexed to a six-layered martensite structure and an intermetallic compound, Ni_3Sn. Corresponding bright field TEM image of the heavily twinned martensite is shown in Fig. 7(b) and the SAED pattern of the martensite is shown in Fig. 7(c). The presence of five satellite spots between principal reflections is consistent with the six-layered structure [33].

4. Thermal characterization

The results of DSC measurements carried out to determine the structural transformation temperatures of the alloys are shown in Fig. 8. Exothermic and endothermic peaks are seen corresponding to the forward and reverse martensitic transformation. There are however no peaks seen for alloys sintered at 950°C shown in brown colour. This indicates that the sintering temperature (950°C) is not adequate to induce reactions which may cause martensitic

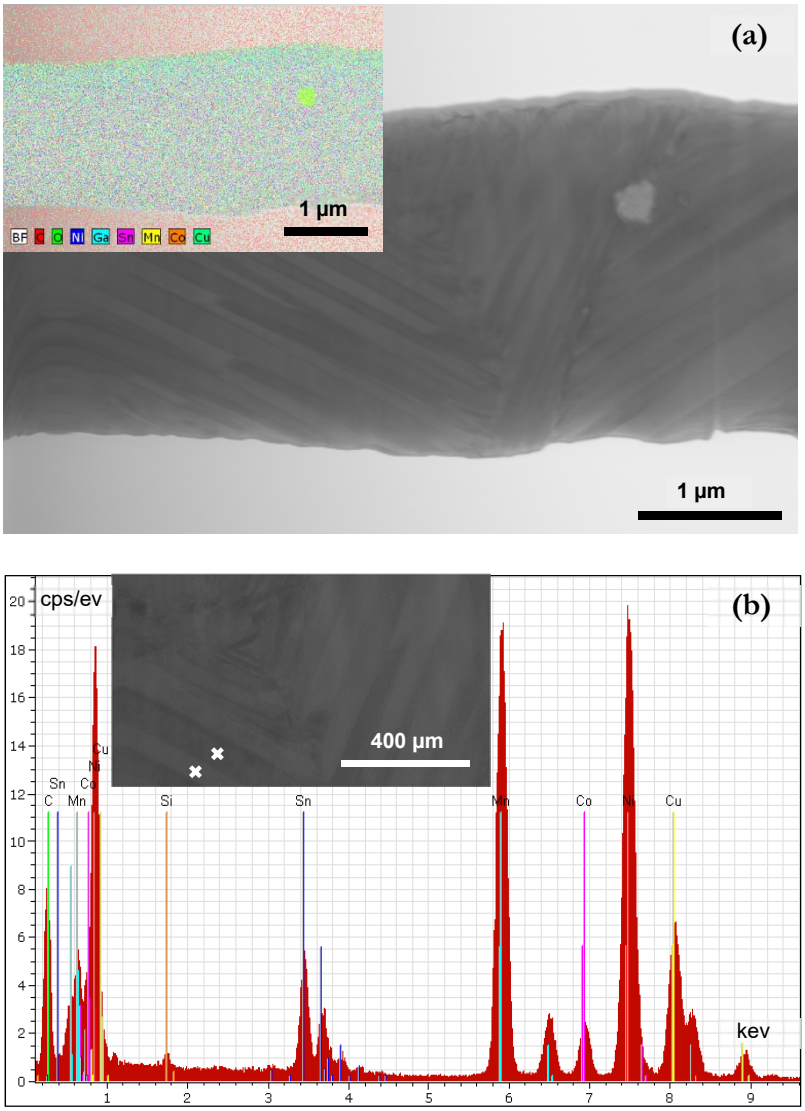

Fig. 6. TEM and compositional map of the as-sintered specimen (a) Martensite grains. Inset shows the map of constituent elements. The presence of Ga is due to ion sputtering during TEM specimen preparation (b) EDS spectrum of marked points on the martensitic laths within the grains, shown in inset.

transformation to occur. For the alloys sintered at 1050°C the austenite start and finish (A_s and A_f, A_f shown) temperatures, as well as the martensitic start and finish temperatures (M_s and M_f, M_s shown), are given in Table 5. A thermal hysteresis of ~25°C is observed. The transformation temperatures are higher when compared to the cast alloys [13], probably due to the presence of Cu in the alloys [34, 35].

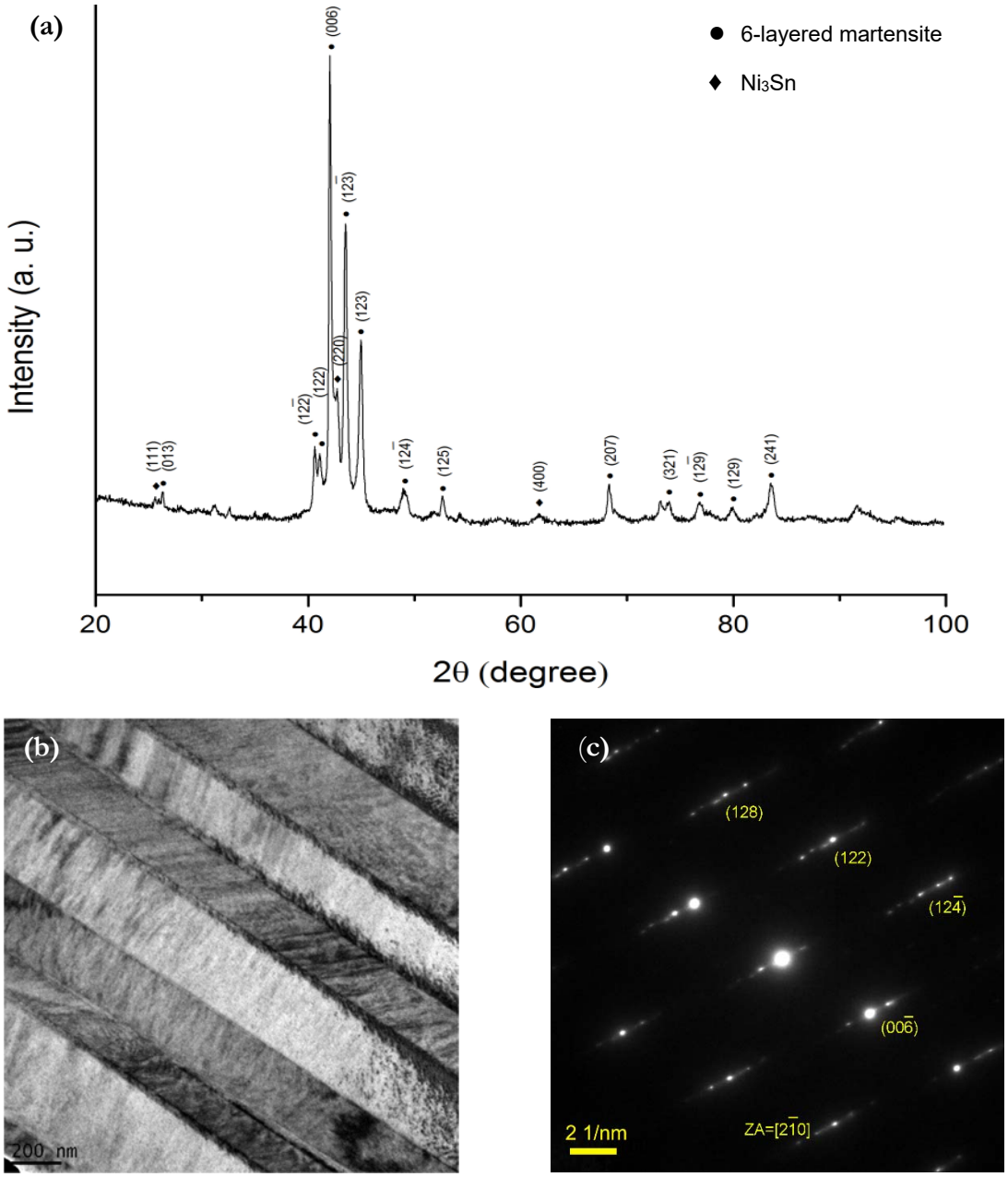

Fig. 7. (a) XRD spectrum of the alloy showing a 6-layered martensite structure and Ni_3Sn phase (b) Bright field TEM image of martensite phase (c) SAED pattern revealing 6-layered martensite.

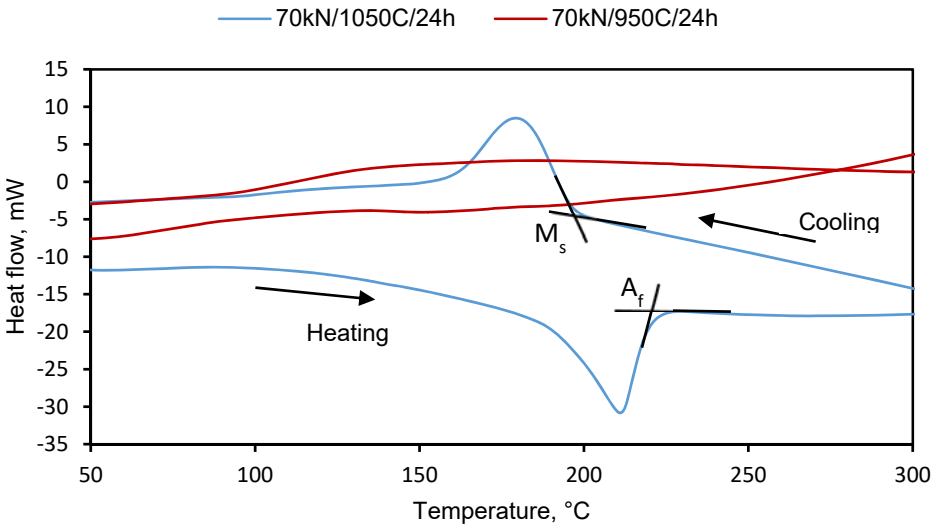

Fig. 8. DSC curves of the alloys sintered at two different temperatures.

Table 5. Phase transformation temperatures.

Alloy	Processing Condition	A_s/°C	A_f/°C	M_s/°C	M_f/°C
1	70/1050/24	188	225	199	159
2	70/950/24	--	--	--	--

5. Magnetisation behaviour

The magnetic transition of the new alloys was characterized from saturation magnetisation (Ms) and ac susceptibility (**χ**) vs temperature (T) measurements using standard protocols in a biased field of 100 Oe in the temperature range of 0 – 400 K. As seen from Fig. 9 a) the magnetisation begins to increase at a temperature in the vicinity of 400 K to ~17 emu/g at 0 K. The Curie temperature could not be clearly established. However it could be inferred that using susceptibility measurements shown in Fig. 9 b) there is a transition from paramagnetic to ferromagnetic behaviour at ~360 K. It is obvious that the martensitic transformation and magnetic transition temperatures are different when compared to the cast alloy in [13]. The decrease in magnetic transition temperatures may be due to the effect of the applied magnetic field which has the effect of decreasing the magnetic transition temperatures in $Ni_{50-x}Co_xMn_{39}Sn_{11}$ multifunctional alloys

when $5 < x < 8$ [34]. Besides as reported in [34] the transformation from martensite to austenite may be field induced. The separation seen between the zero field-cooled and the field-cooled curves may be attributed to the pinning of ferromagnetic domains in different orientations by anti-ferromagnetic exchanges resulting from changes in Mn-Mn spacing introduced by the addition of Sn atoms as suggested in [35]. This may be a further indication that the new alloy sintered has the typical characteristics of a Heusler alloy.

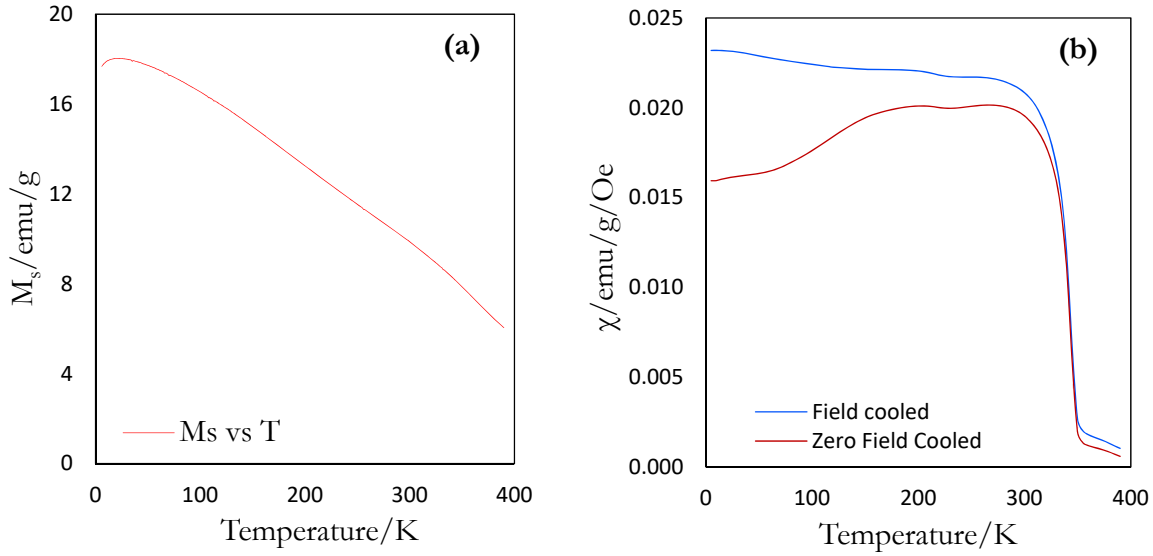

Fig. 9 (a) Temperature vs Magnetisation (b) Temperature vs ac susceptibility curves of the new alloy.

6. Voltage measurement

In order to understand the functional behaviour of the alloy the voltage generated by the alloy as it cooled from different temperatures was measured by means of a simple experiment [36]. The experiment was sufficient to observe the generation of voltage by an identical P/M processed alloy. This reinforces the premise that P/M is a useful tool for the synthesis of ferromagnetic Heusler alloys. The underlying principle of the experiment is based on the fundamental dipolar relationship between magnetization M, magnetic induction B and magnetic field H given by $B = H + 4\pi M$. Since phase deformation has been observed in the alloy it can be assumed to induce a

non-zero dB/dt on which Faraday's law $curl\mathrm{E} = \frac{1}{c}\frac{dB}{dt}$ can be applied as there will be an electromotive force in the coil surrounding the permanent magnet.

Since the phase transformation is reversible, voltage should be generated during both heating and cooling. However the voltage generated during cooling alone was measured and outlined in Table 6. This was due to limitations on the thermal resistance of the material of the device and coil. Furthermore the samples were heated in a furnace to above 400°C and then immediately transferred into the coil. The start temperature listed in the table is the actual temperature at which the voltage measurement was started after the samples were transferred from the furnace. From elemental calculations using the ideas discussed in [37] , the specimen thickness and the coil turns were determined. It can be seen that when the cooling rate is increased with the use of an ice pack, maximum voltage of 0.6 mV is recorded in the specimen with diameter 10 mm and thickness 2 mm, which is exactly the same as in .

The variation of the voltage generated with temperature is plotted in Fig. 10. The time taken for the specimen to cool from 335°C to 50°C is shown in inset. From the voltage plot it can be observed that the maximum voltage of 0.6 mV was generated around 125°C. The martensitic transformation temperature in the case of cast alloy [37] is 135°C. The anomaly is attributed to the composition.

Table 2. Test data

Test start temperature/°C	Method of cooling	Measured voltage/mV	Specimen Diameter/mm	Specimen thickness/mm	Turns of coil
200	Wet pack	0	10	6	4000
220	Wet pack	0.1	10	6	8000
250	Wet pack	0.2	10	2	8000
310	Wet pack	0.4	10	2	8000
335	Ice pack	0.6	10	2	8000

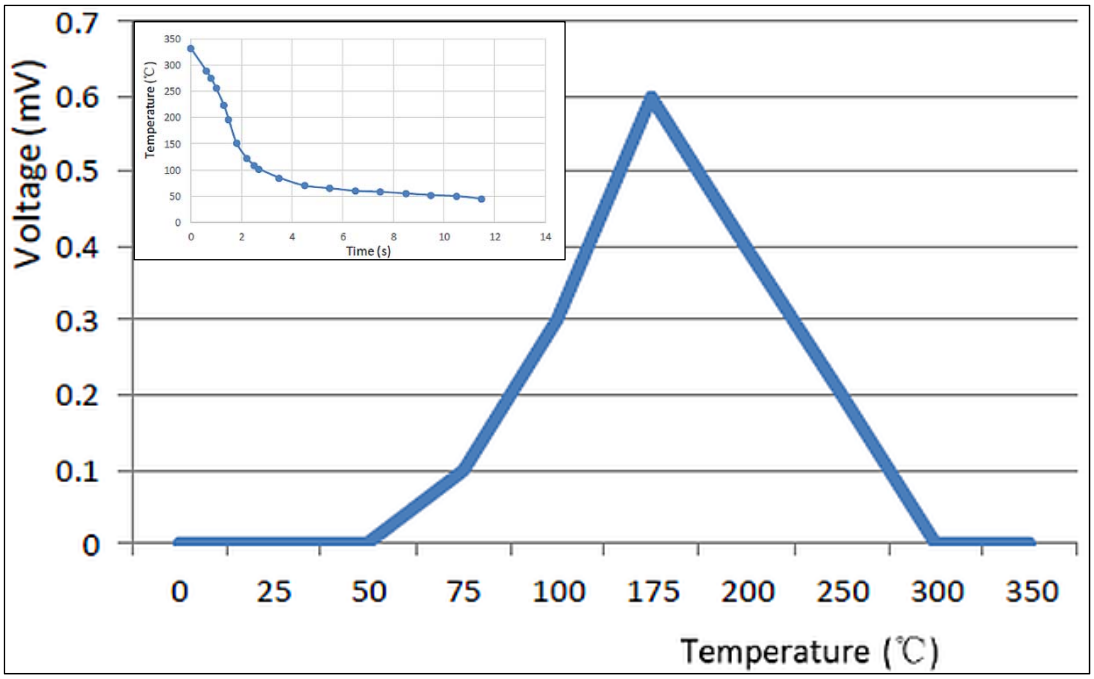

Fig. 10. Voltage generated vs temperature. (Inset) cooling rate of the sample.

7. Conclusions

The Ni-Co-Mn-Sn-Cu quinary alloy was prepared by simple powder metallurgy route in this study. The new findings can be summarised as follows.

1. Synthesis of Ni-Mn based Heusler alloys by powder processing using elemental powders is feasible. A sintering temperature of 1050°C is sufficient for diffusion to occur leading to desired structural transformations. The room temperature microstructure appeared to be a six-layered martensite.
2. The addition of Cu shifted the structural transformation temperature to a higher value, compared to the cast alloys.
3. Magnetic transition from paramagnetic to ferromagnetic occurs at around 360 K (~ 90°C) when a magnetic field of 100 Oe is applied.

Acknowledgements: The authors are grateful to the staff at Adelaide Microscopy for assistance of SEM & EPMA.

8. References

[1] V. Srivastava, K.P. Bhatti. Ferromagnetic shape memory Heusler alloys. in: Hardev Singh Virk, Kleeman W, (Eds.). Ferroics and Multiferroics, vol. 189. Trans Tech Publications Ltd

Switzerland, 2012. pp. 189-208.
[2] R.D. James, Z. Zhang. A way to search for multiferroic materials with "unlikely" combinations of physical properties. in: Manosa L, Planes A, Saxena A, (Eds.). Magnetism and structure in functional materials. Springer, New York, 2005. pp. 159-175.
[3] S.B. Roy. First order magneto-structural phase transition and associated multi-functional properties in magnetic solids, Journal of Physics Condensed Matter 25 (2013).
[4] A. Planes. Controlling the martensitic transition in Heusler shape-memory materials, Physics 3 (2010).
[5] Y. Sutou, Y. Imano, N. Koeda, T. Omori, R. Kainuma, K. Ishida, K. Oikawa. Magnetic and martensitic transformations of NiMnX(X=In, Sn, Sb) ferromagnetic shape memory alloys, Applied Physics Letters 85 (2004) 4358-4360.
[6] S. Aksoy, T. Krenke, M. Acet, E.F. Wassermann, X. Moya, L. Manosa, A. Planes. Magnetization easy axis in martensitic Heusler alloys estimated by strain measurements under magnetic field, Applied Physics Letters 91 (2007).
[7] J.M. Barandiaran, V.A. Chernenko, P. Lazpita, J. Gutierrez, J. Feuchtwanger. Effect of martensitic transformation and magnetic field on transport properties of Ni-Mn-Ga and Ni-Fe-Ga Heusler alloys, Physical Review B 80 (2009).
[8] K. Ullakko, J.K. Huang, C. Kantner, R.C. O/'Handley, V.V. Kokorin. Large magnetic-field-induced strains in Ni2MnGa single crystals, Appl. Phys. Lett. 69 (1996) 1966-1968.
[9] L. Pareti, M. Solzi, F. Albertini, A. Paoluzi. Giant entropy change at the co-occurrence of structural and magnetic transitions in the Ni2.19Mn0.81Ga Heusler alloy, The European Physics Journal B 32 (2003) 303-307.
[10] J. Marcos, A. Planes, L. Manosa, F. Casanova, X. Batlle, A. Labarta, B. Martinez. Magnetic field induced entropy change and magnetoelasticity in Ni-Mn-Ga alloys, Physical Review B 66 (2002).
[11] T. Krenke, E. Duman, M. Acet, E.F. Wasserman, X. Moya, L. Manosa, A. Planes, E. Suard, B. Ouladdiaf. Magnetic superelasticity and inverse magnetocaloric effect in Ni-Mn-In Physical Review B 75 (2007).
[12] K. Koyama, S. Okamoto, T. Watanabe, T. Kanomata, R. Kainuma, W. Ito, K. Oikawa, K. Ishida. Observation of large magnetoresistance of magnetic Heusler alloy Ni50Mn36Sn14 in high magnetic fields, Applied Physics Letters 89 (2006).
[13] V. Srivastava, X. Chen, R.D. James. Hysteresis and unusual magnetic properties in the singular Heusler alloy Ni45 Co5 Mn40 Sn10, Applied Physics Letters 97 (2010).
[14] J.-m. CAO, C.-l. TAN, X.-h. TIAN, Q.-c. LI, E.-j. GUO, L.-p. WANG, Y.-j. CAO. Effect of Co substitution on magnetic properties of Ni-Mn-Sn magnetic shape memory alloys, Transactions of Nonferrous Metals Society of China 24 (2014) 1053-1057.
[15] X. Chen, V.B. Naik, R. Mahendiran, R.V. Ramanujan. Optimization of Ni-Co-Mn-Sn Heusler alloy composition for near room temperature magnetic cooling, Journal of Alloys and Compounds 618 (2014) 187-191.

[16] F. Chen, Y.X. Tong, X.L. Lu, B. Tian, L. Li, Y.F. Zheng. Martensitic transformation and shape memory effect of NiCoMnSn high temperature shape memory alloy, Journal of Materials Engineering and Performance 21 (2012) 2508-2514.
[17] C. Jing, Y.J. Yang, Z. Li, X.L. Wang, B.J. Kang, S.X. Cao, J.C. Zhang, J. Zhu, B. Lu. Tuning martensitic transformation and large magnetoresistance in Ni50−xCuxMn38Sn12 Heusler alloys, Journal of Applied Physics 113 (2013) 173902.
[18] P.O. Castillo-Villa, L. Manosa, A. Planes, D.E. Soto-Parra, J.L. Sanchez-Llamazares, H. Flores-Zuniga, C. Frontera. Elastocaloric and magnetocaloric effects in Ni-Mn-Sn(Cu) shape-memory alloy, Journal of Applied Physics 113 (2013).
[19] M. Kaya, S. Yildirim, E. Yüzüak, I. Dincer, R. Ellialtioglu, Y. Elerman. The effect of the substitution of Cu for Mn on magnetic and magnetocaloric properties of Ni50Mn34In16, Journal of Magnetism and Magnetic Materials 368 (2014) 191-197.
[20] T. Graf, C. Felser, S.S.P. Parkin. Simple rules for the understanding of Heusler compounds, Progress in Solid State Chemistry 39 (2011) 1-50.
[21] C. Suryanarayana. Rapid Solidification Processing. in: Veyssière P, Buschow KHJ, Cahn RW, Flemings MC, Ilschner B, Kramer EJ, Mahajan S, (Eds.). Encyclopedia of Materials: Science and Technology (Second Edition). Elsevier, Oxford, 2002. pp. 1-10.
[22] G.E. Monastyrsky, V. Odnosum, J. Van Humbeeck, V.I. Kolomytsev, Y.N. Koval. Powder metallurgical processing of Ni–Ti–Zr alloys undergoing martensitic transformation: part I, Intermetallics 10 (2002) 95-103.
[23] G.E. Monastyrsky, J. Van Humbeeck, V.I. Kolomytsev, Y.N. Koval. Powder metallurgical processing of Ni–Ti–Zr alloys undergoing martensitic transformation—part II, Intermetallics 10 (2002) 613-624.
[24] S.K. Vajpai, R.K. Dube, P. Chatterjee, S. Sangal. A novel powder metallurgy processing approach to prepare fine-grained Cu-Al-Ni shape-memory alloy strips from elemental powders, Metallurgical and Materials Transactions A: Physical Metallurgy and Materials Science 43 (2012) 2484-2499.
[25] R.B. Perez-Saez, V. Recarte, M.L. No, O.A. Ruano, J.J. San. Advanced shape memory alloys processed by powder metallurgy, Advanced Engineering Materials 2 (2000) 49-53.
[26] A. Ibarra, P.P. Rodriguez, V. Recarte, J.I. Perez-Landazabal, M.L. No, J. San Juan. Internal friction behaviour during martensitic transformation in shape memory alloys processed by powder metallurgy, Materials Science and Engineering A 370 (2004) 492-496.
[27] Y.-W. Kim, Y.-S. Chung, E. Choi, T.-H. Nam. Microstructure and shape memory characteristics of powder-metallurgical- processed Ti-Ni-Cu alloys. vol. 43. 101 Philip Drive, Assinippi Park, Norwell, MA 02061, United States: Springer Boston, 2012. p.2932-2938.
[28] M. Valeanu, M. Lucaci, A.D. Crisan, M. Sofronie, L. Leonat, V. Kuncser. Martensitic transformation of Ti50Ni30Cu20 alloy prepared by powder metallurgy, Journal of Alloys and Compounds 509 (2011) 4495-4498.
[29] K. Ito, W. Ito, R.Y. Umetsu, I. Karaman, K. Ishida, R. Kainuma. Mechanical and shape memory properties of Ni43Co7Mn39Sn11 alloy compacts fabricated by pressureless sintering, Scripta Materialia 63 (2010) 1236-1239.
[30] K. Ito, W. Ito, R.Y. Umetsu, S. Tajima, H. Kawaura, R. Kainuma, K. Ishida. Metamagnetic shape memory effect in polycrystalline NiCoMnSn alloy fabricated by spark plasma sintering, Scripta Materialia 61 (2009) 504-507.
[31] J.A. Monroe, J. Cruz-Perez, C. Yegin, I. Karaman, A.B. Geltmacher, R.K. Everett, R. Kainuma. Magnetic response of porous NiCoMnSn metamagnetic shape memory alloys fabricated using solid-state replication, Scripta Materialia 67 (2012) 116-119.
[32] P.R. Munroe. The application of focused ion beam microscopy in the material sciences, Materials Characterization 60 (2009) 2-13.

[33] L. Righi, P. Lázpita, J. Gutierrez, J.M. Barandiaran, V.A. Chernenko, G. Calestani. Incommensurate 6M-modulated structure of Ni–Fe–Ga martensite, Scripta Materialia 62 (2010) 383-386.
[34] D.Y. Cong, S. Roth, L. Schultz. Magnetic properties and structural transformations in Ni-Co-Mn-Sn multifunctional alloys, Acta Materialia 60 (2012) 5335-5351.
[35] T. Krenke, M. Acet, E.F. Wasserman, X. Moya, L. Manosa, A. Planes. Martensitic transitions and nature of ferromagnetism in the austenitic and martensitic states of Ni-Mn-Sn alloys, Physical Review B

72 (2005).
[36] T. ZHOU, Y. GUO, L. Chen. Waste heat harvesting using multiferroic alloys. Adelaide: The University of Adelaide, 2015.
[37] V. Srivastava, Y. Song, K. Bhatti, R.D. James. The direct conversion of heat to electricity using multiferroic alloys, Advanced Energy Materials 1 (2011) 97-104.